SUPPLEMENTAL DATA

Tunable Protease-Activatable Virus Nanonodes

Justin Judd[1], Michelle L. Ho[1], Abhinav Tiwari[1], Eric J. Gomez[1], Christopher Dempsey[1], Kim Van Vliet[3], Oleg A. Igoshin[1], Jonathan J. Silberg[2], Mavis Agbandje-McKenna[3], Junghae Suh[1*]

[1]Department of Bioengineering, Rice University, Houston, TX USA
[2]Department of Biochemistry and Cell Biology, Rice University, Houston, TX USA
[3]Department of Biochemistry and Molecular Biology, University of Florida, Gainesville, FL USA

*Correspondence should be addressed to J.S. (jsuh@rice.edu). 6100 Main St., MS-142, Houston, TX 77005; T (713)348-2853; F (713)348-5877

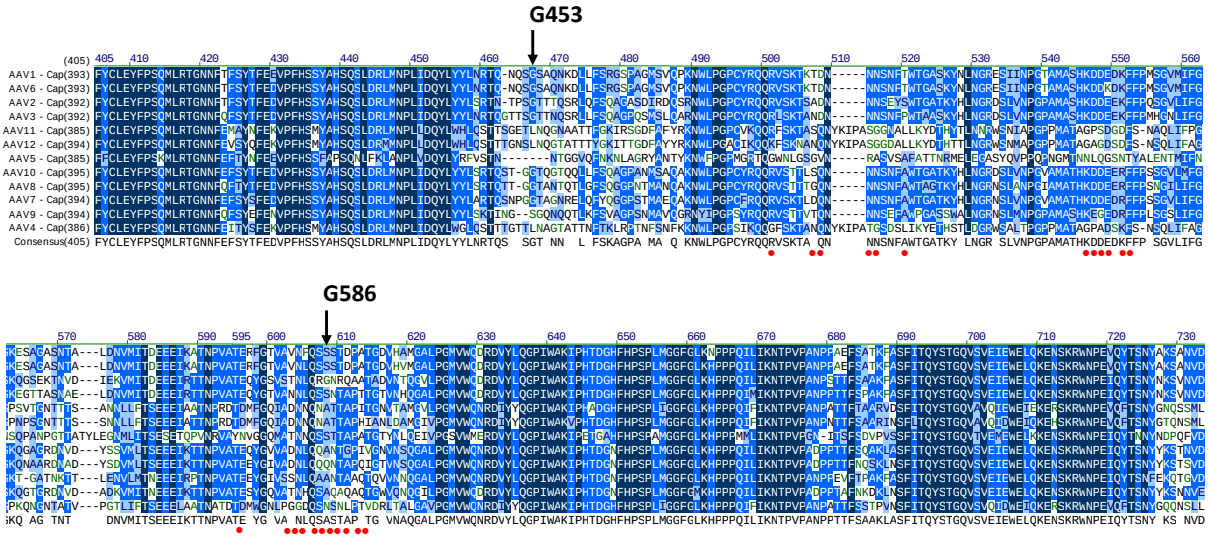

Figure S1. Alignment of AAV capsid serotypes 1-12 show protein context of peptide lock insertions. Sites of insertion, after G453 (top arrow) and G586 (bottom arrow), are indicated. Red dots mark residues in direct contact with bound heparin.[22] Alignment performed in VectorNTI (Life Technologies, Grand Island, NY).

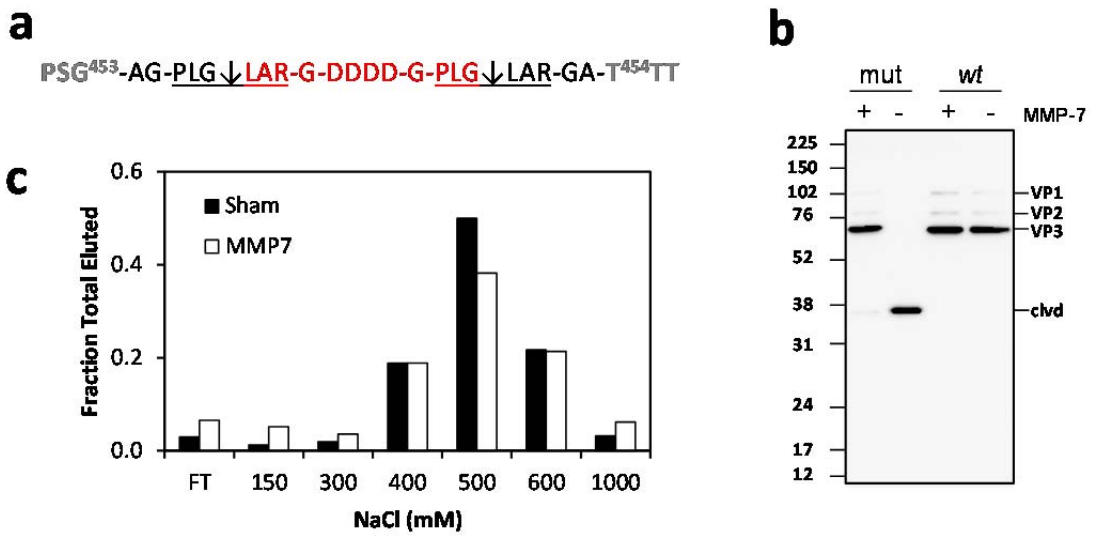

Figure S2. Insertion of Lock1 after G453 (VP1 numbering) fails to regulate AAV-receptor interactions. **a**, Peptide lock (black and red lettering) inserted into AAV2 capsid protein sequence (grey lettering). Scissile bonds are indicated by downward pointing arrows, and red letters indicate peptide removed from capsid. **b,** Western blot of *wt* and mutant capsid proteins after treatment with MMP-7 or a sham buffer, stained with c-terminal specific B1 antibody. The 453 insertion mutant yields intact genome-packaged virions, since blotted samples were isolated from an iodixanol density gradient and could be quantified by qPCR. Western blot shows peptide lock is surface displayed and cleavable by MMP-7, evidenced by truncated cleavage fragment. **c**, However, the inserted peptide fails to regulate AAV-receptor interactions, as heparin affinity chromatography (quantified by qPCR) indicates the mutant retains high affinity for heparin under sham or MMP-7 treatment (both demonstrate peak elution at high salt).

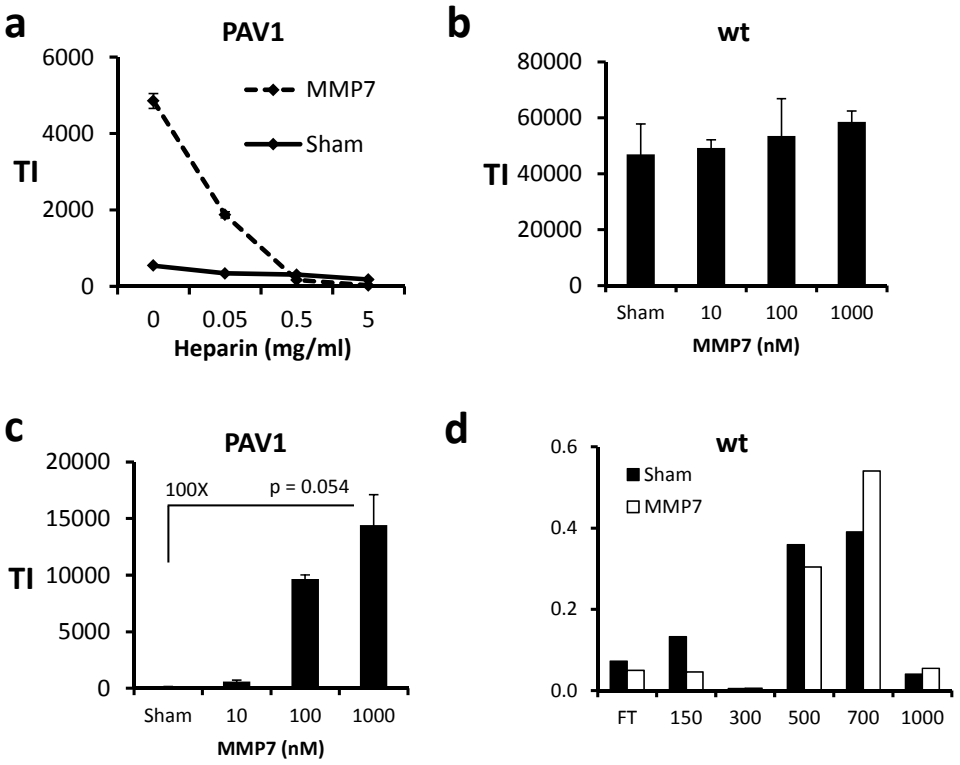

Figure S3. Proteolytic regulation is PAV-specific and heparin-dependent. a, Heparin competition assay indicates activated PAV transduction is heparin-dependent. PAV1 – activated with 100 nM MMP-7 or unactivated with a sham buffer – were incubated with soluble heparin at the indicated concentrations for 1 h. HEK293T cells were then transduced (gMOI = 1000) with treated PAVs and analyzed *via* flow cytometry at 48 h post-transduction. Y-axes indicate transduction index (TI) in all panels. Competing heparin completely abrogates the transduction capacity gained from MMP-7 treatment in activated PAVs. Error bars indicate SEM from a duplicate experiment. **b**, **c**, To show MMP regulation of AAV transduction is specific to PAVs, *wt* capsid AAV2 or PAV1 were treated side-by-side with a sham or increasing concentrations of MMP7. PAV1 experiences > 100-fold increase in activity, whereas the activity of *wt* does not change in response to MMP7 treatment. Error bars indicate SEM (two independent experiments performed in duplicate). **d**, Heparin affinity chromatography demonstrates the affinity of the *wt* AAV2 capsid is unaffected by MMP7 treatment (100 nM), as both yield peak elutions between 500 – 700 mM NaCl, typical of AAV2. All proteolysis experiments were performed at 37 °C for 4 h.

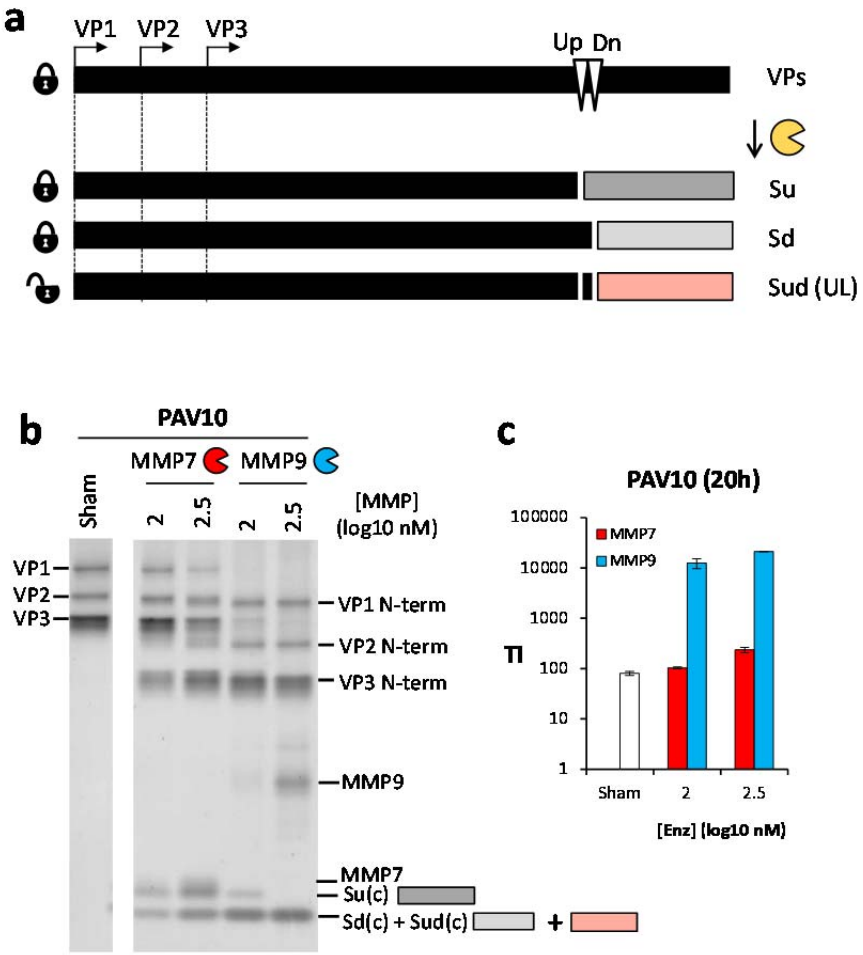

Figure S4. PAV cleavage footprint. a, Scaled schematic showing VP fragments generated by proteolysis. At top, full length VPs -1, -2, and -3 generated from different start sites share overlapping c-terminal protein sequences and differ only by their N-terminal extension (full length VPs -1, -2, and -3 can be seen at top of the sham sample in the gel in **b**, expressed at a typical stoichiometric ratio ~1:1:10, respectively). Proteolysis at the upstream (Up) and downstream (Dn) cleavage sites yields three possible VP cleavage states: 1) S_u, cleaved only at Up, 2) S_d, cleaved only at Dn, and 3) S_{ud}, cleaved at both sites, yielding a fully unlocked VP (UL). Bands containing N- and C-terminal fragments of S_u, S_d, and S_{ud} were used to quantitate PAV1 proteolysis for Fig. 3 (see Figs. S5, S6) **b**, Silver stained 12% polyacrylamide gel of PAV10 digested with indicated concentrations of MMP-7, -9 or a sham for 20 h at 37 °C. MMP-7 appears to exhibit inefficient cleavage at both upsteam and downstream sites (since full length VPs 1, 2, and 3 can be seen at top of the gel and both C-terminal S_u(c) and S_d(c) + S_{ud}(c) fragments can be seen with similarly weak density at bottom). In contrast, MMP-9 reduces all 3 VPs to the corresponding N- and C-terminal fragments, indicating effective proteolysis. Importantly, 2.5 $\log_{10}$ nM MMP-9 condition leads to the disappearance of the S_u(c) fragment, due to complete cleavage of both the upstream and downstream cleavage sites. **c**, PAV10 samples from **b** were used to transduce HEK293T cells (gMOI = 500). Error bars indicate SEM from a duplicate experiment.

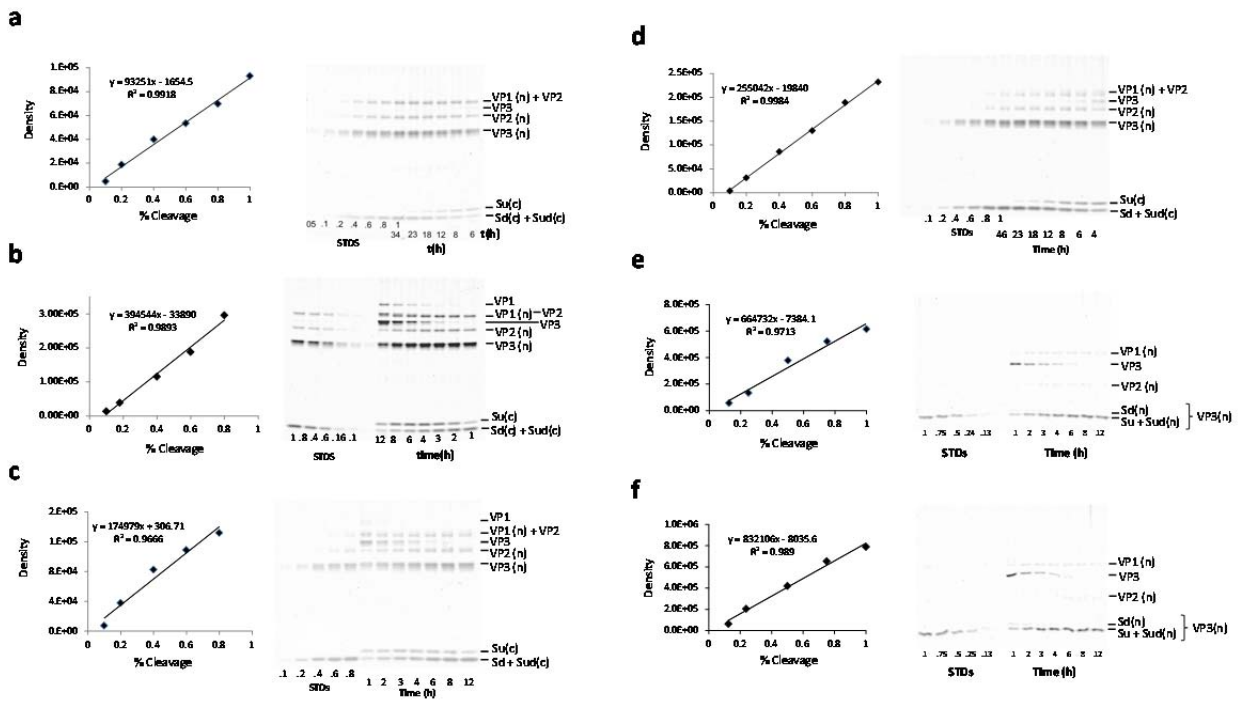

Figure S5. Raw data from kinetic analysis of PAV1 with MMP-9. At left, standard curves generated from densitometric analysis of (**a-d**) smaller C-terminal fragment ($S_d(c) + S_{ud}(c)$) or (**e,f**) smaller N-terminal VP3 fragment ($S_u(n) + S_{ud}(n)$). At right, background-subtracted images used in densitometry. Serial dilutions of the following time points, assumed to represent 100% cleavage, were used to generate STD curves: (**a,b**) 34 h; (**c,d**) 46h; (**e,f**) 1:1 mixture of 34:46h. (**a-d**) N-terminal fragments and native VPs are indicated at top of each image. See Fig. S4 for schematic of C-terminal cleavage fragments from all VPs, and N-terminal cleavage fragments from VP3 start codon.

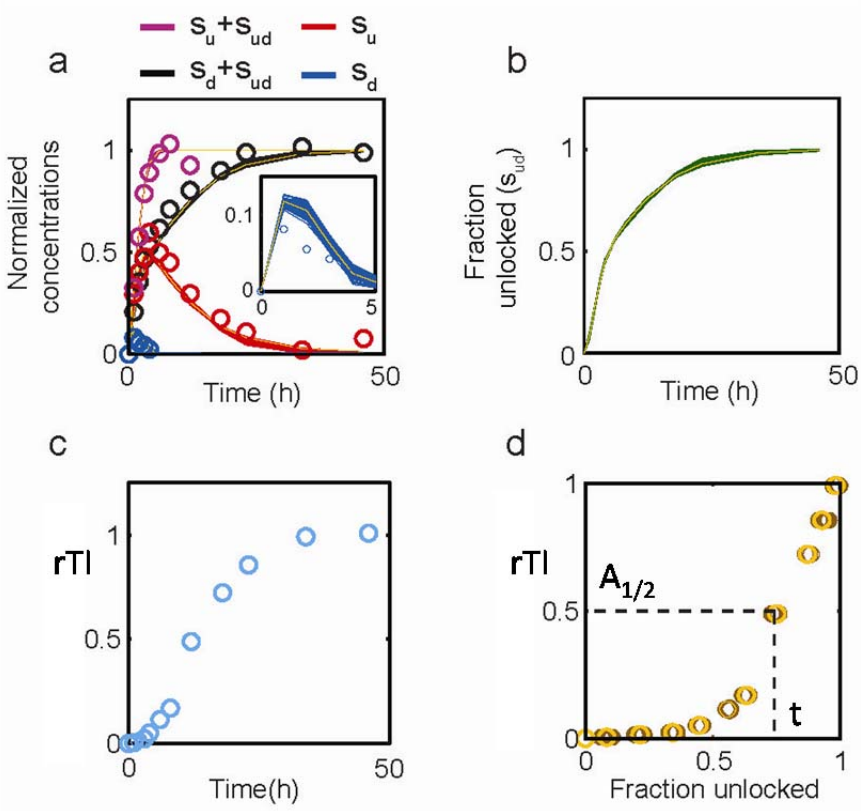

Figure S6. Kinetics of PAV1 capsid cleavage. PAV1 was digested with MMP-9 (100 nM) at 37 °C and stopped at various times. Quantitative silver staining (Fig. S5) was used to measure cleavage over time. **a**, Change in mean densitometric intensity for various proteolytic states (see color legend) plotted versus time. Inset is zoomed in view of S_d. Trajectories obtained from model simulations (curves) were fit to the dynamics data (circles). **b.** Fraction unlocked (UL) dynamics as estimated from the model. Panels **a** and **b** show the top 100 fits (curves) with the best fit shown in yellow. **c**, Virus samples digested for various times were applied to HEK293T cells (gMOI = 1000) to measure virus relative transduction index (rTI, blue circles). **d**, Relative transduction activity (shown in **c**) as a function of fraction unlocked for the top 100 fits (brown circles) with best fit shown in yellow. Threshold (t, dashed line) required to achieve 50% activation ($A_{1/2}$) is shown.

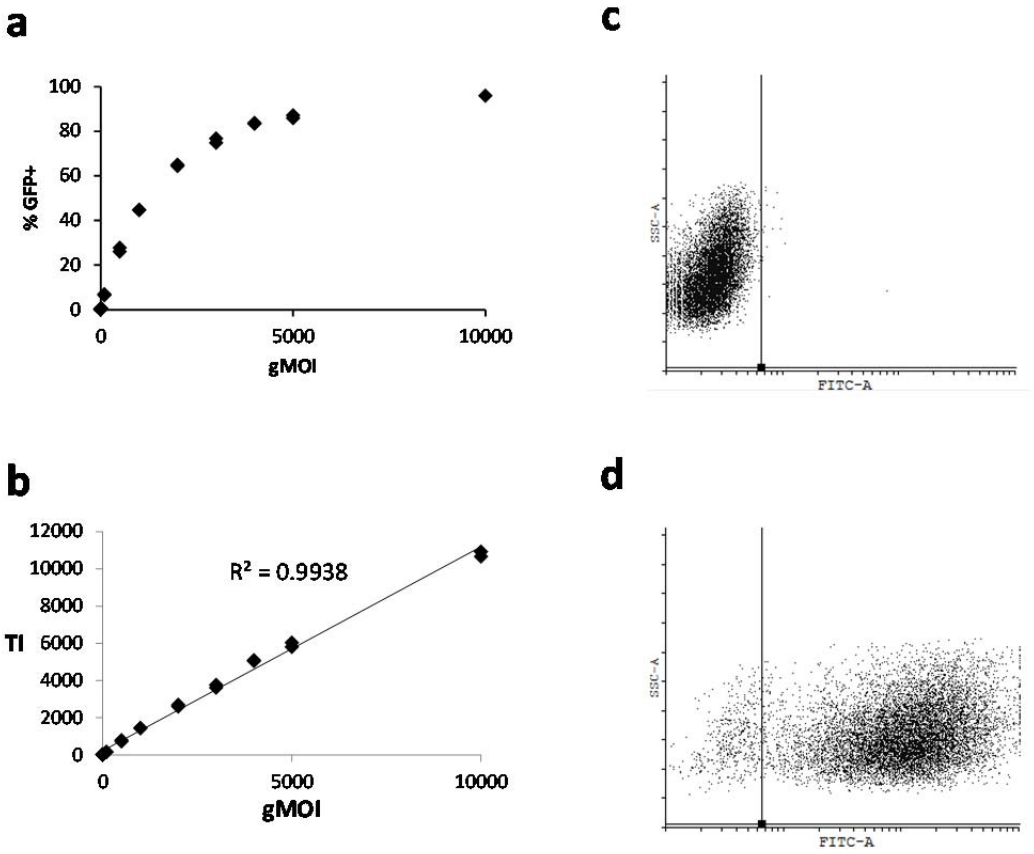

Figure S7. Transduction index (TI) is a linear indicator of virus activity over a wide range of gMOI. HEK293T cells were transduced with *wt* capsid AAV2 (carrying a single stranded GFP transgene) at increasing gMOI, followed by flow cytometric analysis at 48 h post-transduction. **a**, Percent of GFP positive cells becomes non-linear as gMOI increases, since the number of viruses per cell is Poisson distributed with respect to gMOI. **b**, On the other hand, transduction index (TI = % GFP+ cells X geometric mean fluorescence intensity) is linear with respect to gMOI until nearly 100% cells are GFP positive (R^2 = 0.9938). Dot plots **c** and **d** show fluorescence of HEK293T cell populations for gMOI = 0 and 10,000, respectively, from transduction experiment shown in panels **a** and **b**.

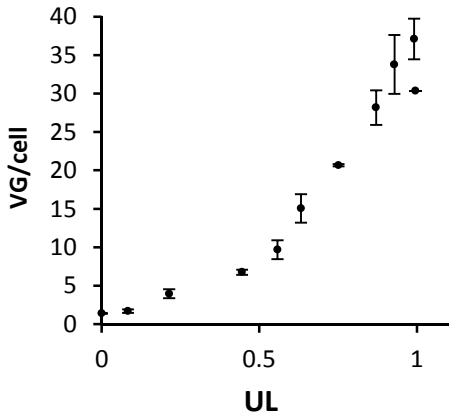

Figure S8. Cellular internalization of PAVs unlocked to different degrees. PAV1, digested with MMP-9 for various times, was applied to HEK293T cells (gMOI = 1000) as in Fig. 3a. After 12 h, cells were washed and harvested by trypsinization. Total DNA was extracted using E.Z.N.A. Tissue DNA kit (Omega Bio-Tek, Norcross, GA) and quantified using a Nanodrop 2000 (Thermo Scientific, Wilmington, DE). Internalized vectors were quantified by qPCR. Y-axis shows vector genomes (VG) per cell, calculated assuming 7 pg genomic DNA per cell. X-axis shows percent unlocked, as calculated in Fig. S6. Error bars are SEM from duplicate experiment.

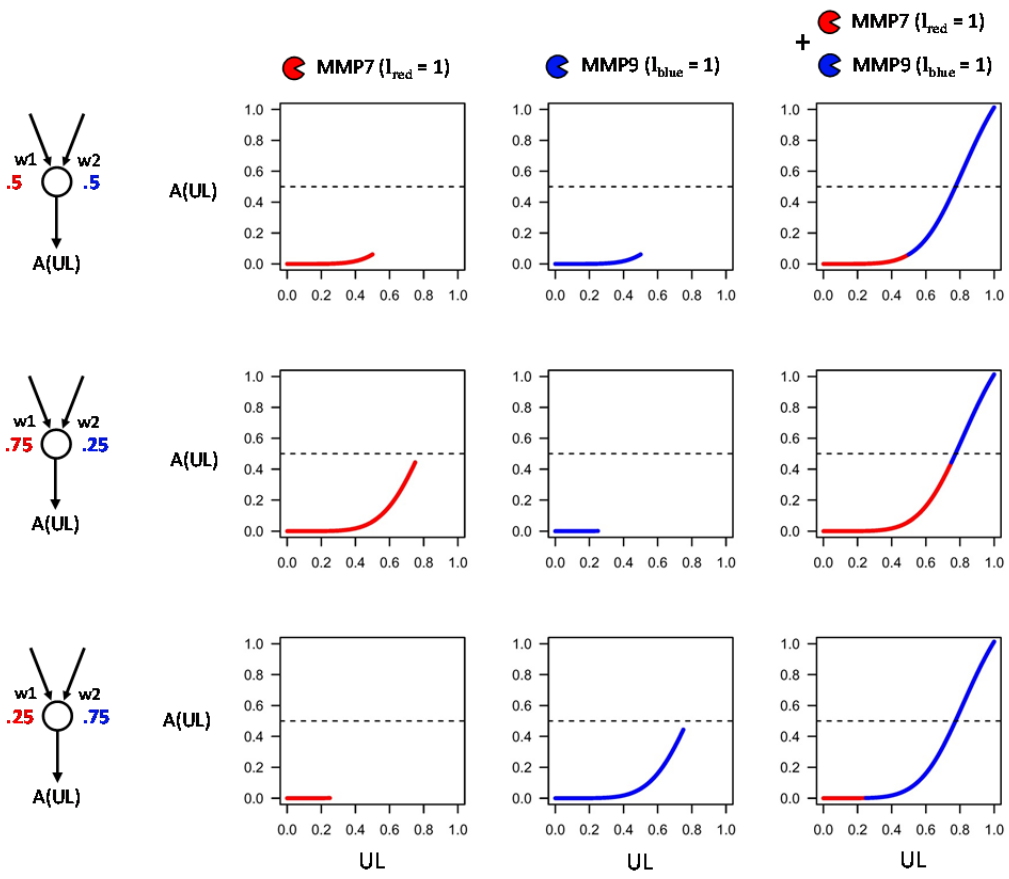

Figure S9. Model predicts AND gate behavior in mosaic PAVs constructed from two highly specific subunits. At left, nodal representations indicate the weights used to construct each of three mosaic PAVs from two hypothetical highly specific subunit types, red and blue, specific for MMP7 and MMP9, respectively. Transfer functions show the predicted analog virus activity A(UL) from such PAVs after complete cleavage of each subunit type by respective proteases separately (left column: I_{red} = 1, I_{blue} = 0; middle column: I_{red} = 0, I_{blue} = 1) and together (right column: I_{red} = 1, I_{blue} = 1). Digitized AND gate behavior is seen in all three hypothetical mosaic PAVs, since the arbitrary activation threshold (dotted line) is only reached when both inputs are active. However, the 0.5/0.5 weighted PAV is predicted to perform optimally, since it has very low activity in response to either protease alone.

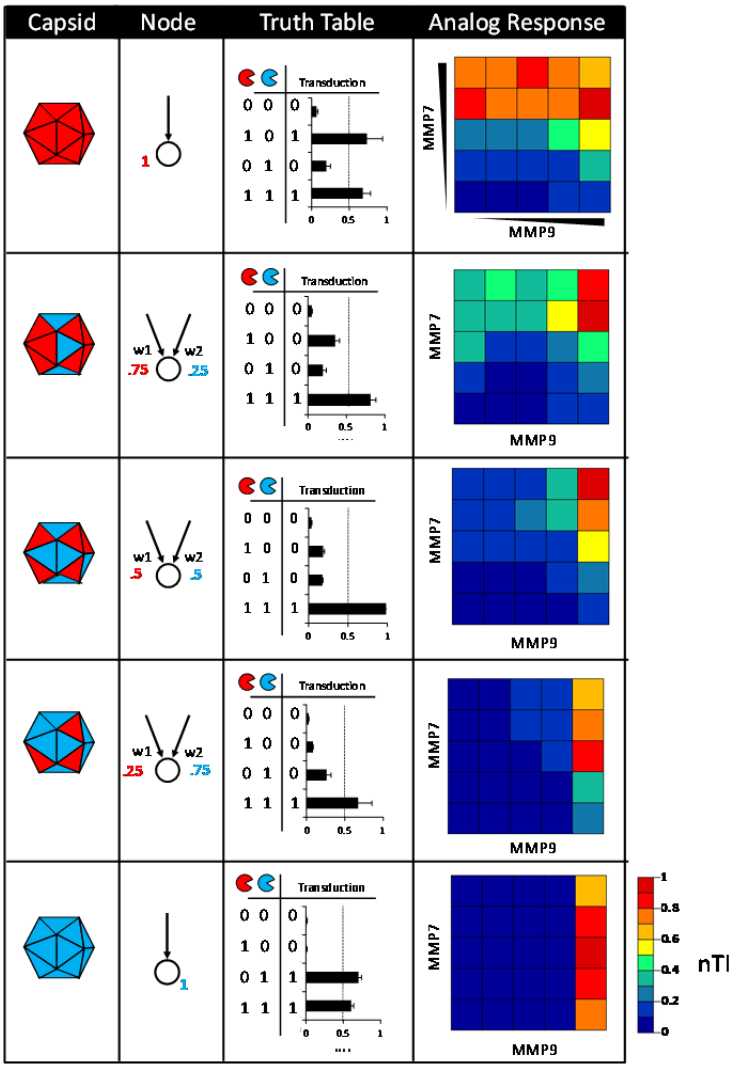

Figure S10. Unzeroed data corresponding to Figure 4. Bar graphs and heat maps report virus activity in units of nTI.